Magnetic Properties and Large-Scale Synthesis of Novel Carbon Nanocomposites via Benzene Decomposition over Ni Nanoparticles

ARTICLE *in* THE JOURNAL OF PHYSICAL CHEMISTRY C · JANUARY 2009

Impact Factor: 4.77 · DOI: 10.1021/jp807898t

Magnetic Properties and Large-Scale Synthesis of Novel Carbon Nanocomposites via Benzene Decomposition over Ni Nanoparticles

Xiaosi Qi,[†] Meihua Xu,[†] Wei Zhong,*[,†] Xiaojuan Ye,[†] Yu Deng,[†] Chaktong Au,[‡] Changqing Jin,[†] and Youwei Du[†]

Nanjing National Laboratory of Microstructures and Jiangsu Provincial Laboratory for NanoTechnology, Nanjing University, Nanjing 210093, People's Republic of China, and Chemistry Department, Hong Kong Baptist University, Hong Kong, People's Republic of China

Received: September 5, 2008; Revised Manuscript Received: December 11, 2008

Nanorods composed of carbon nanoflakes have been synthesized via catalytic decomposition of benzene at temperatures as low as 350 °C over Ni nanoparticles derived from sol−gel synthesis followed by hydrogen reduction. Field-emission scanning electron microscopic and high-resolution transmission electron microscopic images reveal that the carbon nanoflakes are tightly stacked. We investigated the effects of reaction temperature and catalyst amount on the yield, morphology, and magnetic properties of the products. Above 500 °C, the main product was carbon nanotubes. After optimization of reaction parameters, the maximum purity and yield of carbon nanoflakes at 460 °C were 97.9 wt % and ca. 4579% whereas those of nanotubes at 550 °C were 96.7 wt % and ca. 2892%, respectively. Compared to the methods reported in the literature, the approach described herein has the advantages of being simple, low-cost, and environmentally friendly and is suitable for the mass production of one-dimensional carbon nanocomposites that contain magnetic nickel nanoparticles.

Introduction

Over the past decade, attention has been focused on one-dimensional (1-D) carbon nanomaterials such as carbon nanotubes (CNTs), carbon nanofibers (CNFs), and carbon nanocoils (CNCs). Because of their unique physical and chemical properties, the materials can be utilized in areas such as hydrogen storage[1] and absorption and filtration of electromagnetic waves.[2,3] It has been reported that carbon nanomaterials can also be used as catalyst supports, strengthening fibers, etc.[4] By means of wet chemical insertion, capillary suction, in situ arc discharge, and catalyzed hydrocarbon decomposition, foreign materials can be encapsulated inside CNTs. There are potentially wide applications of carbon nanospecies decorated with magnetic materials. For example, it is envisaged that magnetic CNTs in the form of capsules or nanosubmarines can be used in the delivery of drugs to a desired location in a human body.[5]

In general, metal powders of transition elements such as Fe, Co, and Ni are used as catalysts in the synthesis of 1-D carbon nanomaterials. For improvement of activity, oxides such as Al_2O_3, SiO_2, TiO_2, and zeolite are often adopted as catalyst supports. In many applications, removal of catalyst and support materials from the carbon products are necessary,[6] and the process(es) could be tedious and costly. Also, if the purification conditions were harsh, damage of nanomaterials could occur (such as surface modification and formation of structural defects). Furthermore, it is not desirable to synthesize carbon nanomaterials at high temperatures (i.e., above 650 °C),[7−15] because the chance of having other carbon entities as impurities is high. For low-cost generation of high-purity carbon nanomaterials, we need a low-temperature route that involves a support-free catalyst that gives high yield. In previous publications, we reported the synthesis of double helical carbon nanofibers (H-CNFs) and nanotubes (H-CNTs) by the decomposition of acetylene at 450 °C over Fe nanoparticles generated by means of a combined sol−gel/reduction method.[16] A relatively high magnetization value is observed over double H-CNFs and H-CNTs due to the Fe nanoparticles encapsulated at the nodes of the carbon nanomaterials. Recently, we reported the structure of plate-like carbon nanocoils (CNCs) synthesized via acetylene decomposition over Ni nanoparticles at 415 °C. By regulating the temperature for the reduction of the NiO catalyst precursor and that for acetylene decomposition, the CNC yield as well as selectivity to plaitlike and/or single CNCs could be controlled.[17]

The use of aromatic compounds as raw materials for the production of 1-D carbon species has been reported before. Fan et al. synthesized multiwalled CNTs (average diameter 30 nm) from benzene at 1200 °C via a floating catalyst method.[18] Yang et al. reported high production of quasi-aligned CNTs (maximum yield of high-quality CNTs per hour greater than 350%) by catalytic decomposition of benzene at 650 °C.[19] Ruitao et al. synthesized FeNi-filled CNTs from chlorine-substituted benzene at 860 °C.[20] Using carbon materials such as xylene, cyclohexane, camphor, hexane, toluene, pyridine, and benzene, Mahanandia et al. prepared aligned arrays of CNTs at 700 °C.[21] In terms of large-scale production of CNTs, investigations at high temperatures are many but those at low temperatures (below 600 °C) are few.

Large carbon rods are cheap to produce and are widely used as anodic materials of batteries.[22] They have large discharge capacity, small irreversible capacity, high Coulombic efficiency, and low discharge potential for obtaining high voltage. It is hence meaningful to generate and to study miniature carbon rods of nanosize. The carbon nanorods (CNRs) fabricated by us are composed of carbon nanoflakes, and despite the low temperatures, the nanomaterials are polycrystalline. They may be used in areas such as catalysis, hydrogen storage, and miniature cells as well as in absorption and filtration of electro-

* Corresponding author. E-mail: wzhong@mail.nju.edu.cn.
[†] Nanjing University.
[‡] Hong Kong Baptist University.

10.1021/jp807898t CCC: $40.75
Published on Web 01/20/2009

magnetic waves. Until now, most of the published works on the generation of carbon nanomaterials via the catalytic decomposition of organic compound have focused on CNTs rather than on CNRs.[23−27] Herein, we report the low-temperature synthesis of CNRs (with high yield and high purity) over Ni nanoparticles (no support) derived from a sol−gel method followed by in situ hydrogen reduction. The approach is highly reproducible: the maximum purity and yield of CNRs are ca. 97.9 wt % and ca. 4579%, respectively. To the best of our knowledge, the synthesis of CNRs composed of carbon nanoflakes from benzene over Ni nanoparticles has never been reported before.

Experimental Section

To prepare the NiO catalyst precursor, 0.03 mol of $NiCl_2 \cdot 6H_2O$ and 0.045 mol of citric acid monohydrate were well mixed with 300 mL of absolute ethanol, and the mixture was stirred at 60 °C for 6 h. With the evaporation of ethanol at 80 °C and heating of the residue at 500 °C in air for 4 h, the xerogel turned to NiO. Then 0.03 g of the NiO powder was spread on a ceramic plate placed inside a reaction tube. In order to obtain high-purity carbon nanomaterials in a large quantity, a quartz tube that was 6 cm in diameter and 80 cm in length (equipped with temperature and gas-flow controls) was used as the reactor. Subsequently, the NiO powder was in situ reduced to Ni nanoparticles under H_2 at 500 °C for 4 h. After NiO reduction, benzene (in a three-necked flask maintained at 70 °C over a water bath) was carried into the reaction tube by a flow of argon. The decomposition of benzene was conducted at a designated temperature for 6 h at atmospheric pressure over the Ni nanoparticles. The "as-obtained" product (black in color) was collected after cooling to room temperature (RT). Hereinafter, the samples synthesized at 350, 460, and 550 °C are denoted as C-350, C-460, and C-550, respectively.

The samples were examined on an X-ray powder diffractometer (XRD) at RT for phase identification using Cu Kα radiation (Model D/Max-RA, Rigaku, Japan). Raman spectroscopic investigations were performed using a Jobin-Yvon Labram HR800 instrument with 514.5 nm Ar^+ laser excitation. Elemental analysis for carbon, hydrogen, and nitrogen was performed on a CHN-O-Rapid (Heraeus, Germany) instrument. Thermoanalysis was carried out on a thermal analysis system (Perkin-Elmer TGA7 series) with ca. 5.0 mg of sample heated in air at a rate of 10 °C/min. The composition of the samples was analyzed by induced coupled plasma (ICP) spectrometry (Jarrell-Ash, USA). The morphologies of the samples were examined over a transmission electron microscope (TEM) and a high-resolution TEM (HRTEM, Model JEOL-2010, Japan) operating at accelerating voltages of 120 and 200 kV, respectively, and by a field-emission scanning electron microscope (FE-SEM, Model 1530VP, LEO, Germany) operating at an accelerating voltage of 5 kV. The magnetic properties of samples were measured at 300 K using a vibrating sample magnetometer (VSM, Lakeshore, USA). Fourier transform infrared (FTIR) spectroscopy of samples (in KBr pellets) were recorded using a Nicolet 510P spectrometer.

Results and Discussion

Microstructures and Magnetic Properties of As-Prepared CNRs. Using 0.03 g of NiO nanoparticles as catalyst precursor, 0.386 g of CNR sample was generated at 350 °C. The yield (defined as weight ratio of carbon to nickel) was ca. 1537%. The XRD pattern of C-350 is shown in Figure 1a. The diffraction peaks are attributed to (002) and (101) reflections of hexagonal graphite (JCPDS Card File No. 41-1487, lattice parameters $a = 2.470$ Å and $c = 6.756$ Å), and (111) and (200) reflections of cubic Ni^0 (JCPDS Card File No. 01-1258, lattice parameter $a = 3.540$ Å). The outcome of elemental analysis of C-350 showed no indication of hydrogen. Figure 1b shows the IR spectrum of C-350. There are no IR signals of −CH=CH−, $-CH_2-$, and $-CH_3$ entities. Accordingly, we deduce that the method adopted in this study is capable of producing carbon nanomaterials. The thermogravimetric (TG) curve of C-350 shows a weight loss in the temperature range 500−700 °C and a residue of 7.73 wt % (Figure 1c). The loss is ascribed to carbon oxidation and the residue to NiO. The result of ICP analysis indicated that the Ni content in the as-prepared sample was 5.93 wt %, which is close to the 6.07 wt % value deduced from the TG curve. The results indicate that the nickel of the adopted catalyst was part of the C-350 sample.

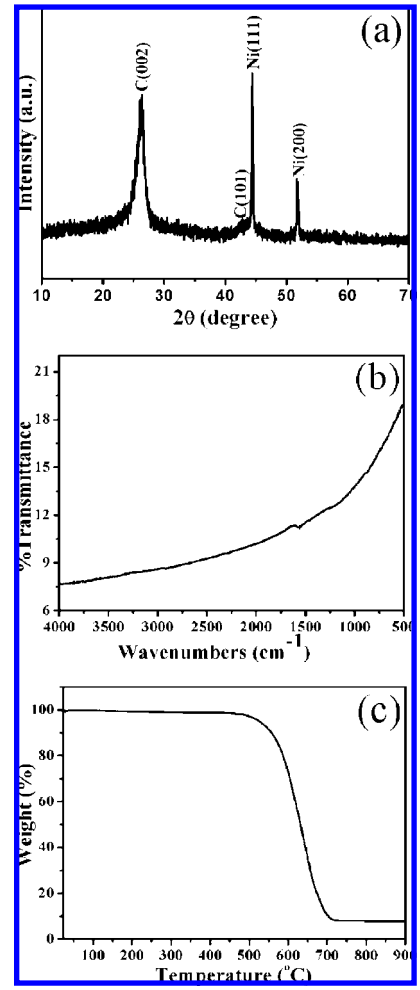

Figure 1. (a) XRD pattern, (b) IR spectrum, and (c) thermogravimetric (TG) curve of C-350.

Figure 2 shows the FE-SEM images of C-350. There are nanorods of several microns in length and 200−400 nm in diameter. From Figure 2b, we can distinctly observe that the CNRs are composed of nanoflakes. It is known that interaction between graphitic layers is weak, and we envisage that rupture of the CNRs should be easy. We find "clear-cut" ends of CNRs different from those of CNTs, CNCs, and CNFs, and attribute the phenomenon to the fracture of flake-composed CNRs. Based on the FE-SEM images, we estimated a CNR selectivity of ca. 90%; the rest are coiled nanowires and nanotubes of irregular morphology.

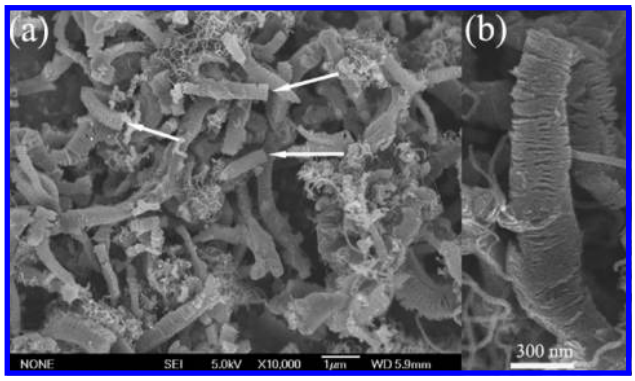

Figure 2. FE-SEM images of C-350 at (a) low and (b) high magnification. The arrows indicate the "clear-cut" ends of CNRs.

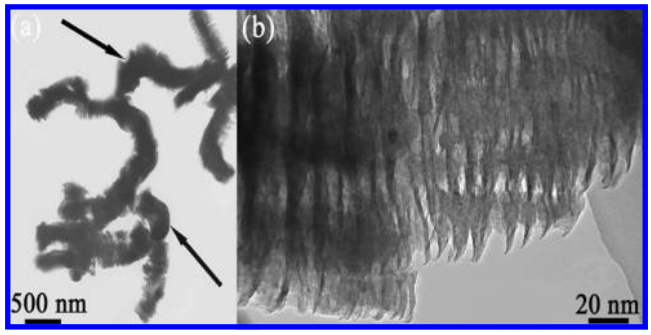

Figure 3. (a) TEM and (b) HRTEM images of C-350. The arrows indicate Ni nanoparticles.

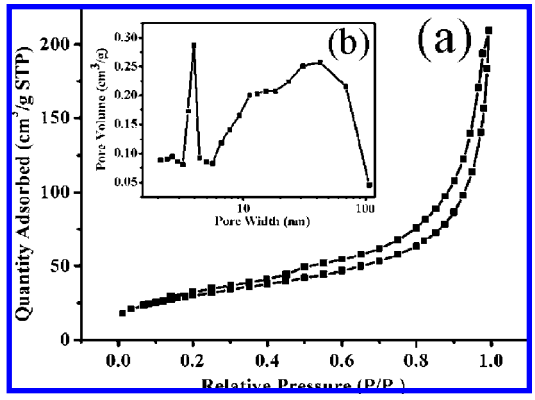

Figure 4. (a) N_2 adsorption and desorption isotherms, and (b) pore size distribution of C-350.

Shown in Figure 3a is a TEM image typical of C-350. The Ni nanoparticles indicated by arrows (Figure 3a) have a grain size of ca. 200 nm, slightly smaller than the diameter of CNRs. The distribution of Ni nanoparticles in CNRs is not uniform. Due to the easy rupture of flake-composed CNRs, there are sections of CNRs that do not show any presence of Ni nanoparticles. Figure 3b shows the HRTEM image of the nanoflakes. It is noted that the flakes are closely stacked. There are gaps between the flakes, but no doubt there are also contacts. We have performed an extensive TEM investigation on the CNR samples, and we found that over 90% of carbon species are CNRs composed of nanoflakes.

Figure 4 depicts the N_2 adsorption and desorption isotherms and pore size distribution of C-350. According to IUPAC classification, the hysteresis loop can be denoted as type H3, indicative of the existence of slitlike pores associated with aggregates of platelike particles.[28,29] The result is in harmony with the nanoflake-stacked structure of C-350. The Brunauer–Emmet–Teller (BET) surface area of the material is 109.28 m^2/g. According to the Barrett–Joyner–Halenda (BJH) approach,[30] we obtained the pore size distribution. Shown in Figure 4b is the differential pore volume as a function of pore diameter. There is a narrow peak around 4 nm and a broad one stretching from 6 to 100 nm. The average pore size of C-350 is 11.19 nm.

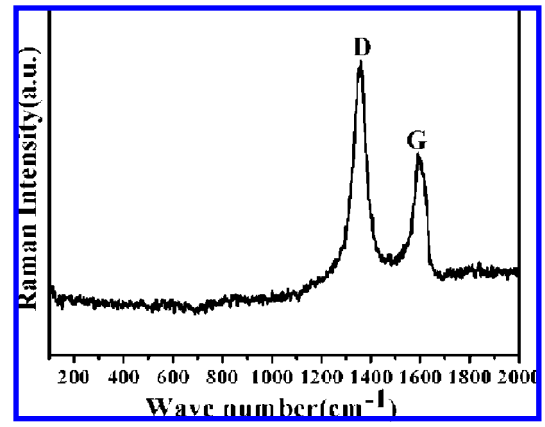

Figure 5. Raman spectrum of C-350.

Raman spectroscopy is an important tool for studying carbon nanomaterials, and information related to crystal structure and disorder can be obtained.[31–33] In general, the Raman band in the 1500–1605 cm^{-1} region is noted as the G-band (graphite band) and that in the 1250–1450 cm^{-1} region is the D-band (disorder band). The G-band is related to the C–C vibration of the carbon material with sp^2 orbital structure,[34] indicative of graphitic layers of high crystallinity caused by the tangential stretching modes (graphitic lattice mode E_{2g}).[35] The D-band is the disorder-induced phonon mode that is related to the mode of boundaries in the Brillouin zone. It is due to the disorder components and mainly originates from the phonon mode of the M-point and the K-point of the hexagonal Brillouin zone. The Raman spectrum (Figure 5) of C-350 exhibits two peaks: one at ca. 1352 cm^{-1} and the other at ca. 1600 cm^{-1}. The detection of the D-band with a broad half-width of 105.1 cm^{-1} confirms the presence of disorder and/or distortion in the CNR sample. The intensity ratio of the D-band and the G-band (i.e., I_D/I_G) is commonly used to characterize the crystallinity of carbon materials. In our study, an I_D/I_G of ca. 1.31 was recorded for C-350, implying the presence of defects. It is understandable because the temperature for benzene decomposition was relatively low. We deduce that, besides the formation of graphitic carbon, there is the generation of amorphous carbon during the decomposition of benzene.

Magnetic properties of C-350 were investigated at RT. As illustrated in Figure 6, the C-350 sample reaches magnetic saturation rapidly and a small hysteresis loop can be observed as depicted in the inset of Figure 6. The saturation magnetization (M_S) and coercivity (H_C) at RT are 3.10 emu g^{-1} (1 emu g^{-1} = 1 A m^2 kg^{-1}) and 90.7 Oe (1 Oe = $1000/4\pi$ A m^{-1}), respectively. Based on the Ni content of C-350 (5.93 wt %, based on ICP analysis) and the fact that the magnetization of metallic nickel at RT is ca. 55 emu g^{-1}, we estimate that the M_S of C-350 should be around 3.26 emu g^{-1}, a value not far from the one (i.e., 3.10 emu g^{-1}) observed experimentally. Nevertheless, we detected nonuniformity in magnetic property inside C-350. We divided a batch of C-350 into seven portions and separately measured the M_S of each portion; the highest M_S was 3.37 emu g^{-1} whereas the lowest was 2.65 emu g^{-1}, showing a mean value of 2.99 emu g^{-1} (root-mean-square error 0.23 emu g^{-1} and relative error 7.69%). The results show that

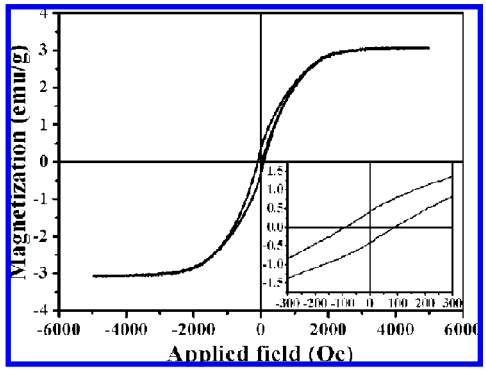

Figure 6. Typical magnetization curves measured at RT over C-350. The inset shows enlarged parts of the curves close to the origin.

the Ni particles are not evenly distributed throughout the batch of C-350, in accord with the result of TEM observation (Figure 3a). We tested a C-350 sample that had been exposed to air for over 6 months and found no changes in XRD features and magnetic properties. The high stability of Ni nanoparticles in ambient environment could be a result of Ni entrapment inside the flake layers. Overall, we find that the C-350 sample is stable in air and shows relatively high magnetization due to the ferromagnetic Ni nanoparticles. To the best of our knowledge, such a kind of magnetic CNR species (with nanoflake structure) has never been reported before.

Effects of Benzene Decomposition Temperature. In this study, the effects of benzene decomposition temperature on the morphology, yield, and magnetic properties of carbon nanomaterials were also investigated. We found that the decomposition temperature has distinct influence on the morphology as well as on the yield of the carbon products. At a decomposition temperature of 460 °C, ca. 1.103 g of CNRs is collected in each run; the C-460 yield is ca. 4579% and the carbon purity is up to 97.9 wt %. As shown in Figure 7a, the residue attributed to NiO (left after TG analysis) is ca. 2.53 wt %. The X-ray diffraction pattern of C-460 shows only the diffraction peaks of hexagonal graphite and cubic Ni^0 (Figure 7b). Compared to C-350 (Figure 1a), the C-460 sample shows weaker Ni^0 signals and a bigger lattice parameter (*c*) (6.804 versus 6.756 Å), indicating that the distance between graphitic layers in CNRs was enlarged with the rise of reaction temperatures. The results of ICP analysis revealed that the Ni content in C-460 is 2.09 wt % (versus 5.93 wt % in C-350). The Raman spectrum of C-460 (Figure 7c) is similar to that of C-350 (Figure 5), except that there is an increase in G-band intensity (relative to that of D-band, $I_D/I_G = 1.18$). The results indicate that the C-460 sample is lower in Ni content but better in graphite crystallinity. Figure 7d shows the magnetization−coercivity curves of C-460. The M_S of C-460 is 1.01 emu g^{-1}, markedly smaller than that of C-350, plausibly due to the lower content of Ni in C-460.

Figure 8 shows FE-SEM images of C-460. With a change of decomposition temperature from 350 to 460 °C, there is an increase of CNR yield but a change in CNR morphology: the nanorods of C-460 become curly in shape and bigger in diameter (ca. 500 nm). From Figure 8b, one can clearly see that the curly nanorods are also composed of carbon nanoflakes.

According to the FE-SEM and HRTEM images of C-550, the majority of carbon species generated in the decomposition of benzene are multiwalled CNTs with inner diameter ca. 5 nm and outer diameter ranging from 15 to 40 nm (Figure 9a,b); the selectivity to CNTs is high, up to ca. 88%. The interplanar distance of the graphitic layers is ca. 0.34 nm. It is clear that the CNTs are polycrystalline. The average pore size and BET

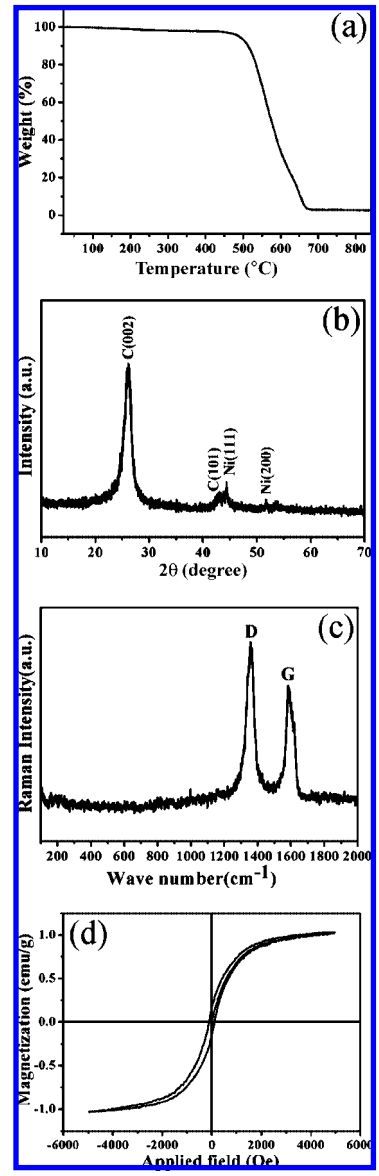

Figure 7. (a) TG curve, (b) XRD pattern, (c) Raman spectrum, and (d) magnetization curves of C-460.

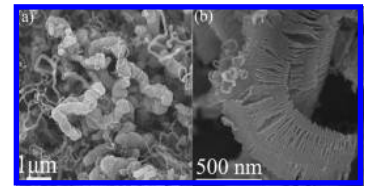

Figure 8. FE-SEM images of C-460 sample at (a) low and (b) high magnification.

surface area of C-550 are 9.42 nm and 105.58 m^2/g, respectively. From the TEM image shown in Figure 9c, uneven distribution of Ni nanoparticles is apparent. The Ni nanoparticles are not wrapped at a particular location of CNTs; they may be located at the middle or wrapped at the nozzles of the tubes. The weight of C-550 obtained over a 30 mg NiO precursor catalyst was ca. 0.682 g in each run, corresponding to a carbon yield of ca. 2793% and carbon purity of ca. 96.5 wt %. It is clear that one can synthesize CNRs or CNTs selectively by regulating the temperature for benzene decomposition. It is possible that the yield of a particular nanomaterial can be optimized within a certain range of temperature. We divided the C-550 sample into

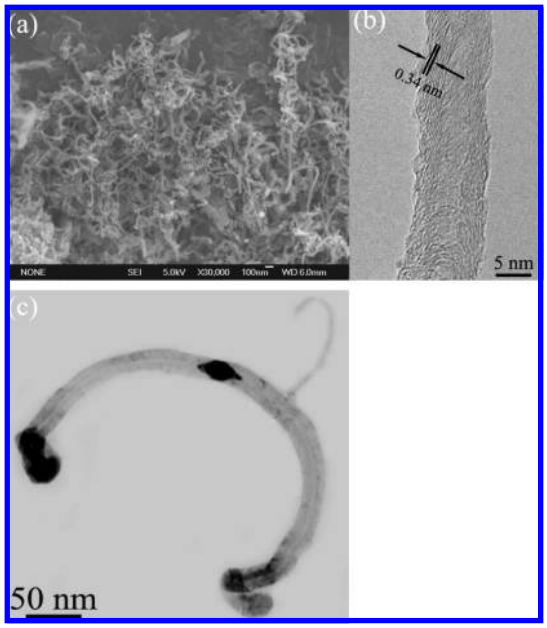

Figure 9. (a) FE-SEM, (b) HRTEM, and (c) TEM images of C-550.

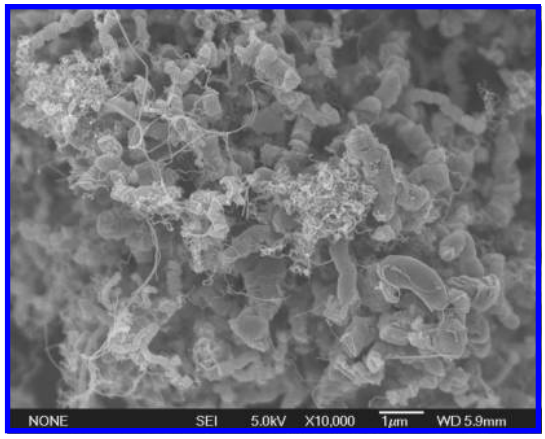

Figure 10. Typical FE-SEM image of the sample obtained at benzene decomposition temperature of 460 °C when 50 mg of NiO was used as catalyst precursor.

five portions and separately measured the M_S of each portion (not shown). The results also reveal an uneven distribution of Ni particles within the sample. We recorded a mean M_S value of 1.73 emu g^{-1} (root-mean-square error 0.19 emu g^{-1} and relative error 10.98%).

Effect of Catalyst Amount. We found that the amount of NiO catalyst precursor used has a profound influence on the morphology and yield of carbon products. If the temperature for benzene decomposition was 460 °C and the amount of NiO was 50 mg rather than 30 mg (see Experimental Section) and the other conditions remained unchanged, the product in each run was ca. 0.847 g and the yield of carbon species was 2156%; compared to a yield of 4579% as in the case of 30 mg of NiO, the decrease in yield is significant. As shown in the FE-SEM image (Figure 10), there is a small population of coiled fiberlike carbon species. Based on the results, we deduce that the amount of catalyst used has a determining effect on CNR selectivity and yield. It is believed that, by increasing the amount of catalyst, one can enhance the rate of benzene decomposition. We suggest that, by adopting an appropriate amount of catalyst, one can achieve maximum generation of CNRs.

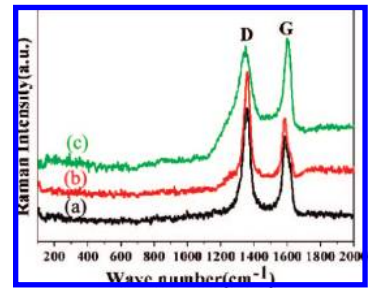

Figure 11. Raman spectrum of C-460: (a) as-prepared, (b) heated in air at 300 °C for 6 h, and (c) heated in Ar at 750 °C for 4 h.

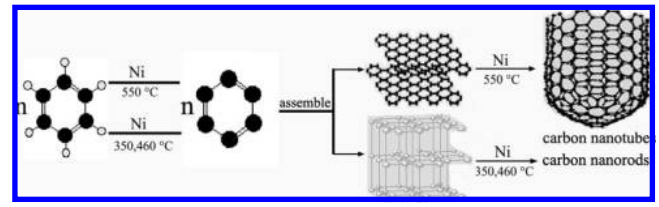

Figure 12. Proposed formation mechanism of CNTs and CNRs.

Thermal Stability in Air or Argon. We heated the C-460 sample in air at 300 °C for 6 h or in argon at 750 °C for 4 h and detected no significant change in XRD pattern and in TEM morphology (not shown). Figure 11 shows the Raman spectrum of C-460 and that of the thermally treated samples. We find no significant discrepancy between the Raman profile of as-prepared C-460 and that of the one thermally treated in air at 300 °C. However, after a 4-h thermal treatment in argon at 750 °C, there is a significant decline in I_D/I_G (0.94). It is clear that, by annealing the C-460 sample in argon at 750 °C, one can raise the graphitization level of CNRs.

Formation Mechanism of CNTs and CNRs. The CNRs composed of carbon nanoflakes as shown in Figures 2b and 3b have not been reported before. The availability of the material could open up a new dimension for the design of miniature devices for electrical applications. The exact mechanism for the formation of carbon nanostructures via catalytic chemical vapor deposition (CCVD) is not well understood. Fan et al. described that the strong interaction (base-growth mode) between support and catalyst would result in the growth of CNTs containing no nanoparticles of the catalyst.[36] Other researchers such as Amelickx et al. believed that, due to weak interaction (tip-growth mode) between support and catalyst, there is entrapment of catalyst nanoparticles at the tube tips.[37] Moreover, Wang et al. proposed a formation mechanism of CNRs over Fe and Ag nanoparticles: nanorods are formed via the assembly of clusters of 1-D conjugate carbon chains originated from free C_2 entities.[23] Based on the model of Gamaly and Ebbesen,[38] Zou et al. suggested that at moderate and low distribution velocities of carbon atoms on catalyst surfaces, CNRs and CNTs are respectively formed.[25] Based on our experimental results and the reported models,[10,25,36−38] we tentatively suggest a mechanism to explain the formation of CNRs and CNTs. According to the TEM images of C-350 (Figure 3a) and C-550 (Figure 9c), there is encapsulation of nickel nanaoparticles at the ends or in the middle of the nanorods and nanotubes. The results suggest that the growth of CNTs and CNRs over the Ni catalyst follows the tip-growth mode. Our proposed mechanism complies with such an understanding (Figure 12). The possible pathway for CNT and CNR growth may be as follows: (i) breakage of all the C−H bonds of benzene, resulting in the formation of hexagonal carbon rings, (ii) assembly of the rings into clusters, followed by the development of graphitic layers at relatively

high temperature (e.g., 550 °C), and (iii) growth of the graphitic layers into nanotubes at active sites of Ni. The rolling up of a graphitic sheet is likely because, at high temperatures in the presence of Ni nanoparticles, the graphitic layers tend to curve up, bringing about the formation of the tube structures. However, below 460 °C, the graphitic layers formed are relatively small in area, and prefer to stack up along the direction normal to the facets of Ni nanoparticles.

Conclusions

In summary, CNRs composed of carbon nanoflakes can be synthesized via a low-temperature (350−460 °C) and environmentally friendly route of catalytic decomposition of benzene over Ni nanoparticles. Above 500 °C, the major product is multiwalled CNTs. In terms of CNRs or CNTs, the yield as well as the kind of products can be controlled by regulating the temperature for benzene decomposition. A relatively high magnetization value is observed over CNRs due to the entrapment of Ni nanoparticles inside the carbon flakes. The CNR material is thermally stable in air at 300 °C and in argon at 750 °C. Thus we have reported a simple and cost-effective way for the large production of CNRs and CNTs that show unique magnetic properties.

Acknowledgment. This work was supported by the National Natural Science Foundation of China (Grant 10674059) and the National Key Project for Basic Research (Grant 2005CB623605), People's Republic of China.

References and Notes

(1) Furuya, Y.; Hashishin, T.; Iwanaga, H.; Motojima, S.; Hishikawa, Y. *Carbon* **2004**, *42*, 331.
(2) Motojima, S.; Hoshiya, S.; Hishikawa, Y. *Carbon* **2003**, *41*, 2658.
(3) Xie, G. W.; Wang, Z. B.; Cui, Z. L.; Shi, Y. L. *Carbon* **2005**, *43*, 3181.
(4) Zhang, G. Y.; Jiang, X.; Wang, E. G. *Appl. Phys. Lett.* **2004**, *84*, 2646.
(5) Korneva, G.; Ye, H. H.; Gogotsi, Y.; Halverson, D.; Friedman, G.; Bradley, J. C.; Kornev, K. G. *Nano Lett.* **2005**, *5*, 879.
(6) Vivekchand, S. R. C.; Jayakanth, R.; Govindaraj, A.; Rao, C. N. R. *Small* **2005**, *1*, 920.
(7) Jang, J. W.; Lee, K. W.; Oh, I. H.; Lee, E. M.; Kim, I. M.; Lee, C. E.; Lee, C. J. *Solid State Commun.* **2008**, *145*, 561.
(8) Chen, Y.; Liu, C.; Du, J. H.; Cheng, H. M. *Carbon* **2005**, *43*, 1874.
(9) Sung, W. Y.; Ok, J. G.; Kim, W. J.; Lee, S. M.; Yeon, S. C.; Lee, H. Y.; Kim, Y. H. *Nanotechnology* **2007**, *18*, 245603.
(10) Jehng, J. M.; Tung, W. C.; Kuo, C. H. *J. Porous Mater.* **2008**, *15*, 43.
(11) Piedigrosso, P.; Konya, Z.; Colomer, J. F.; Fonseca, A.; Tendeloo, G. V.; Nagy, J. B. *Phys. Chem. Chem. Phys.* **2000**, *2*, 163.
(12) Sarangi, D.; Karimi, A. *Nanotechnology* **2003**, *14*, 109.
(13) Xie, J. N.; Mukhopadyay, K.; Yadev, J.; Varadan, V. K. *Smart Mater. Struct.* **2003**, *12*, 744.
(14) Cheng, J. P.; Zhang, X. B.; Tu, J. P.; Tao, X. Y.; Ye, Y.; Liu, F. *Mater. Chem. Phys.* **2006**, *95*, 12.
(15) Ivanov, V.; Fonseca, A.; Nagy, J. B.; Lucas, A.; Lambin, P.; Bernaerts, D.; Zhang, X. B. *Carbon* **1995**, *33*, 1727.
(16) (a) Tang, N. J.; Zhong, W.; Gedanken, A.; Du, Y. W. *J. Phys. Chem. B* **2006**, *110*, 11772. (b) Tang, N. J.; Zhong, W.; Au, C.; Gedanken, A.; Yang, Y.; Du, Y. W. *Adv. Funct. Mater.* **2007**, *17*, 1542.
(17) Tang, N. J.; Zhong, W.; Gedanken, A.; Du, Y. W. *J. Phys. Chem. C* **2008**, *112*, 10061.
(18) Fan, Y. Y.; Li, F.; Cheng, H. M.; Su, G.; Yu, Y. D.; Shen, Z. H. *J. Mater. Res.* **1998**, *13*, 2342.
(19) Yang, Y.; Tian, Y. J.; Lü, Y. N.; Wang, X. Z.; Chen, Y. *Nanotechnology* **2003**, *14*, 733.
(20) Ruitao, Lv.; Kang, F. Y.; Wang, W. X.; Wei, J. Q.; Gu, J. L.; Wang, K. L.; Wu, D. H. *Carbon* **2007**, *45*, 1433.
(21) Mahanandial, P.; Nanda, K. K. *Nanotechnology* **2008**, *19*, 155602.
(22) Yoon, S. H.; Park, C. W.; Yang, H. W.; Korai, Y.; Mochida, I.; Baker, R. T. K.; Rodriguez, N. M. *Carbon* **2003**, *42*, 21.
(23) Wang, X. J.; Lu, J.; Xie, Y.; Du, G. A.; Guo, Q. X. *J. Phys. Chem. B* **2002**, *106*, 933.
(24) Mannsberger, M.; Kukovecz, A.; Georgakilas, V.; Rechthaler, J.; Hasi, F.; Allmaier, G.; Prato, M.; Kuzmany, H. *Carbon* **2004**, *42*, 953.
(25) Zou, G. F.; Lu, J.; Wang, D. B.; Xu, L. Q.; Qian, Y. T. *Inorg. Chem.* **2004**, *43*, 5432.
(26) Xia, Y. D.; Yang, Z. X.; Mokaya, R. *Chem. Mater.* **2006**, *18*, 140.
(27) Liu, Q.; Liu, W.; Cui, Z. M.; Song, W. G.; Wan, L. J. *Carbon* **2007**, *45*, 268.
(28) Sing, K. S. W.; Everett, D. H.; Haul, R. A. W.; Moscou, L.; Piterotti, R. A.; Rouquerol, J.; Siemieniewska, T. *Pure Appl. Chem.* **1985**, *57*, 603.
(29) Rouquerol, J.; Avnir, D.; Fairbridge, C. W.; Evertt, D. H.; Haynes, J. H.; Pernicone, N.; Ramsay, J. D. F.; Sing, K. S. W.; Unger, K. K. *Pure Appl. Chem.* **1994**, *66*, 1739.
(30) Barrett, E. P.; Joyner, L. G.; Halenda, P. P. *J. Am. Chem. Soc.* **1951**, *73*, 373.
(31) Dresselhaus, M. S.; Dresselhaus, G.; Jorio, A.; Filho, A. G. S.; Saito, R. *Carbon* **2002**, *40*, 2043.
(32) Thomas, J. M. *Carbon* **1969**, *7*, 359.
(33) Lefrant, S.; Baltog, I.; Baibarac, M.; Schreiber, J.; Chauvet, O. *Phys. Rev. B* **2002**, *65*, 235401.
(34) Ivanov, V.; Fonseca, A.; Nagy, J. B.; Lucas, A.; Lambin, P.; Bernaerts, D.; Zhang, X. B. *Carbon* **1995**, *33*, 1727.
(35) Xie, S. S.; Li, W. Z.; Pan, Z. W.; Chang, B. H.; Sun, L. F. *Eur. Phys. J. D* **1999**, *9*, 85.
(36) Fan, S.; Chapline, M. G.; Franklin, N. R.; Tombler, T. W.; Cassell, A. M.; Dai, H. *Science* **1999**, *283*, 512.
(37) Amelickx, S.; Zhang, X. B.; Bernaerts, D.; Zhang, X. F.; Ivanov, V.; Nagy, J. B. *Science* **1995**, *267*, 635.
(38) Gamaly, E. G.; Ebbesen, T. W. *Phys. Rev. B* **1995**, *52*, 2083.

JP807898T